Composites Science and Technology 258 (2024) 110870

Contents lists available at ScienceDirect

Composites Science and Technology

journal homepage: www.elsevier.com/locate/compscitech

Effect of atomic oxygen and vacuum thermal aging on graphene and glass fibre reinforced cyanate ester-based shape memory polymer composite for deployable thin wall structures

Sandaruwan Jayalath [a,b,c], Eduardo Trifoni [d], Jayantha Epaarachchi [a,b,*], Madhubhashitha Herath [a,e], Eleftherios E. Gdoutos [f,g], Bandu Samarasekara [h]

[a] Centre for Future Materials & Institute of Advanced Engineering and Space Sciences, University of Southern Queensland, Toowoomba, Australia
[b] School of Engineering, Faculty of Health, Engineering and Sciences, University of Southern Queensland, Toowoomba, Australia
[c] Division of Polymer and Chemical Engineering Technology, Institute of Technology University of Moratuwa, Diyagama, Homagama, Sri Lanka
[d] School of Astronomy and Astrophysics, Australian National University, Canberra, Australia
[e] Department of Engineering Technology, Faculty of Technological Studies, Uva Wellassa University, Badulla, Sri Lanka
[f] Graduate Aerospace Laboratories, California Institute of Technology, Pasadena, CA, 91125, USA
[g] Proteus Space, Inc., Los Angeles, CA, 90021, USA
[h] Department of Material Science and Engineering, University of Moratuwa, Sri Lanka

ARTICLE INFO

Handling Editor: Dr. Ming-Qiu Zhang

Keywords:
Deployable thin wall structures
Durability of shape memory polymer composites
High-temperature applications
Load-bearing applications
Shape memory polymer composites

ABSTRACT

Deployable components and structures are a crucial part of space exploration. Due to fewer parts, low weight and cost, shape memory polymers (SMPs) and their composites (SMPCs) are considered ideal candidates for this. However, lower thermal stability and poor durability in the space environment have limited their applicability. This research work details the development of Graphene Nanoplatelets (GNP) filled Glass Fibre (GF) reinforced cyanate ester-based SMPC with 0/90° and ±45° sandwich fibre lay-up configuration capable of multidirectional shape programming. The SMP matrix was synthesised by mixing Cyanate Ester and Polyethylene Glycol (PEG) with added GNP. SMPC was fabricated by pouring the SMP mixture into a pre-prepared glass mould with the added GF layers. The synthesised SMPC showed shape programming and recovery at 169.01 ± 0.62 °C and stable thermomechanical properties at the temperature of 130 °C. Durability tests at extreme environmental conditions including Atomic Oxygen exposure, thermal vacuum aging, and elevated-temperature behaviour tests were conducted as these tests evaluate the durability and applicability of the SMPC for use in Earth's orbits and lunar environments. The performances of the samples before and after durability tests were measured through mechanical tests, shape memory effect tests and a series of characterisation methods such as microscopic image analysis, FTIR and dynamic mechanical analysis. According to the results, AO exposure affected the SMPCs by eroding their surface. There were no changes in the chemical structure of the SMPC yet the thermomechanical, mechanical and shape memory properties were decreased without compromising their safe operational levels such as storage onset temperatures (128.79 ± 3.08 °C), maximum tensile stress (114.99 ± 21.52 MPa), shape fixity (100 %) and recovery ratios (100 %). The erosion resistance of the GNP-filled SMPCs was improved with ~54.35 % less erosion than the SMPC without GNP. The vacuum thermal aging slightly slowed shape recovery from 31.17 % to 8.32 % at 160 °C due to PEG crosslink degradation, however, 100 % shape recovery was achieved at the end. Further durability tests under cryogenic temperatures and effects after vacuum thermal cycles are warranted to observe the synergistic effect on the SMPC for future developments. Exploring the scalability and additive manufacturability of the developed SMPC can be advantageous in the future while mitigating challenges such as complex shape programming, long-term materials degradation, resource efficiency and compliance with safety standards.

* Corresponding author. School of Engineering, Faculty of Health Engineering and Sciences, University of Southern Queensland, Toowoomba, 4350, QLD, Australia.
E-mail address: Jayantha.Epaarachchi@unisq.edu.au (J. Epaarachchi).

https://doi.org/10.1016/j.compscitech.2024.110870
Received 12 June 2024; Received in revised form 12 September 2024; Accepted 17 September 2024
Available online 19 September 2024

1. Introduction

Since the beginning of smart material inventions, shape memory polymers (SMPs) have become an integral branch of smart material-based application developments [1]. Their ability to be programmed into complex shapes and recover back to their original shape by affecting the polymeric structure using external stimuli such as—heat, light, electricity, moisture and magnetism [2–5] has distinguished them from other smart materials. Furthermore, the availability of synthesised SMPs in a plethora of thermo-mechanical properties, mechanical properties, durability levels, densities and shapes has made them ideal candidates for numerous applications such as deployable structures [6,7], bio-medical devices [8], satellite components [9] and aerospace components [10]. With the recent developments of high-performing SMPs such as—polyimide [11], isopthalamide (MPA) [2] and cyanate ester [12] based SMPs with high-temperature resistance, irradiation resistance and additive manufacturing capability have paved the path to developing space-related applications in recent years. Most of the SMP-based deployable components for space applications are used in microgravity environments where operational loads of the structures are insignificant and therefore no strength requirement for significant mechanical properties [13,14] of the SMP material. In a study done by Higgins M. et al. (2020) [15], it was determined that pursuing a hybrid concept of inflatable and rigid habitats will be more desirable after comparing a number of concepts according to their features such as shapes, launch mass/volume, ease of construction, expandability and maintenance. Therefore, the development of a space-grade SMP that can bear applied operational loads fills the gaps in future requirements such as deployable dwelling units and modular habitats on the moon and the other planets.

The extraterrestrial environment, commonly referred to as outer space, presents formidable challenges. Despite its harsh conditions, human-made objects not only survive but also flourish in various orbits [16], including low earth orbit (LEO), medium earth orbit (MEO) and geostationary orbit (GEO). Furthermore, ambitious plans are underway to establish a lunar base, marking a significant leap towards our cosmic exploitation including the Artemis mission by NASA. Both LEO and Lunar environments reach +120 °C and +125 ± 2 °C of high temperatures as well as −120 °C and −173 °C of cryogenic temperatures, respectively [17,18]. Apart from that, short and long thermal cycles, high vacuum, atomic oxygen exposure in LEO, and charged particle exposure in Lunar, UV and Gamma radiation are relatively common conditions in LEO and Lunar environments. While LEO objects experience 16 thermal cycles a day, Lunar objects experience 1 thermal cycle over 28 day period with 14 days of sun and 14 days of nights [17–20]. Due to these reasons, an SMP that needs to be used in LEO or Lunar conditions must go through intensive durability testing to be a useable material.

Even with the recent developments in new grades of SMPs, the inherited weak mechanical properties of polymers are often mitigated by adding reinforcing fillers and fibres [21–24]. A recent book chapter by Gowri M. et al. (2022) [25] Further, discusses the reinforcement of composite materials with both natural and synthetic fibres enhancing the mechanical properties of SMPs. This makes the shape memory polymer composites (SMPCs) suitable for load-bearing and structural applications. However, the lower mechanical properties of the SMPs and SMPCs at elevated temperatures limit their ability to be used in above mentioned environments. To qualify for the deployable components or structures, an SMP should have higher activation temperatures, stable thermo-mechanical properties at elevated temperatures, low outgassing, high fracture toughness and most importantly durability in extreme environments. Cyanate ester is a well-developed grade of advanced thermoset polymer that consists of the above-mentioned space-worthy properties [26,27]. It has undergone several accelerated aging tests such as vacuum outgassing, vacuum UV radiation exposure, atomic oxygen exposure and vacuum thermal cycles under space conditions and survived [28–32]. The robustness of Cyanate ester SMPs has been extensively discussed in recent reviews by the leading author [27,33].

This research work focuses on using cyanate ester SMP developed by the authors (Jayalath S. et al. (2024) [34]) and fabricating a glass fibre-reinforced SMPC for the development of load-bearing structural components for LEO or lunar-related applications. Among reviewed high-performing SMPs such as Epoxy, Polyimide, Styrene and Cyanate ester-based SMPs, Cyanate ester and Polyimide have gone through the NASA-STD-6001 materials for spacecraft tests and passed. They also have shown the best thermomechanical properties over 200 °C and the best radiation resistance. Availability, cost, ease of synthesis and low toxicity of BACE were considered as the major factors selected for this study. Compared to readily used carbon, aramid, and basalt fibres, the inherited flexibility of glass fibres has given freedom to the SMPCs to be programmed and recovered efficiently [35]. Graphene Nanoplatelets were used as a nanofiller to increase the thermal conductivity of the shape memory properties since both cyanate ester and glass fibres are less effective in heat conduction. The SMPC that has been developed in this study can maintain its storage modulus stable over the highest temperatures at LEO and Lunar environments. The shape memory effect (programming and recovery) takes place at Tan(δ) peak temperature (T_δ) enabling the SMPC to serve its design purpose effectively. This is due to the increased rubbery properties of the polymer over its storage onset temperature. Furthermore, SMPC is fabricated with 0/90° and ±45° glass fibre sandwich layer configuration (TX) to support multidirectional stresses and shape programming [36]. The effect of adding GNP as a thermal filler is also tested during this study. As per the durability evaluation, SMPCs were tested under 48 h of AO exposure, 4 weeks of vacuum thermal aging and up to 140 °C of elevated temperatures. Finally, suitability analysis was done by calculating the dimensions of a hemispherical dish-ended thin wall pressure vessel using the SMPC parameters in the worst-case scenario.

The development of this SMPC that can withstand multi-directional stresses, extreme environmental conditions and thermo-mechanical stability at high temperatures is a game-changing material for multiple applications. Load-bearing components in orbital satellites (switches, hinges, and truss booms), as well as deployable thin shell structures (dwelling units and modular habitats for space and the moon), can be mentioned as two key applications.

2. Experimentation

2.1. Materials and specimen preparation

2.1.1. Materials

For the SMP synthesis, the Bisphenol-A cyanate ester monomer (BACE, M_n = 278.31) was acquired from Wenzhou Blue Dolphin New Material Co. Ltd, China. As the shape memory effect modifier, Polyethylene Glycol (PEG, M_n = 600) were supplied from Chem Supply Australia. Graphene Nanoplatelets (GNP) (surface area: 750 g/m^2) were supplied from Sigma-Aldrich Australia and used as a thermal filler in the SMPC. Glass fibre fabric (GF) (plain-weave, 200 g/m^2, ATL Composite, Australia) was used as the reinforcing fibre.

2.1.2. SMP synthesis

SMPs were synthesised with the stochiometric ratios of 9:1 (BACE: PEG) aiming to achieve storage onset glass transition temperature (T_g) around 130 °C. All the chemicals were used as received. BACE and PEG mixture was fully melted at 90 °C and 0.6 *wt*% of GNP was added and then mixed using a probe sonicator (Bandelin SONOPLUS 200 W, Germany) with 50 % amplitude, 30 s ON and 5s OFF for 20 min keeping the temperature of the mixture above 90 °C. Meanwhile, glass moulds with laid-up glass fibre layers were prepared and a chemical mixture was poured from a side (Fig. 1). Then the mixture was degassed inside a Labec vacuum oven in 11.15 kPa (~89 % vacuum/111.46 mbar) at 100 °C for 30 min. The chemical mixture was cured at 100 °C for 3 h, at

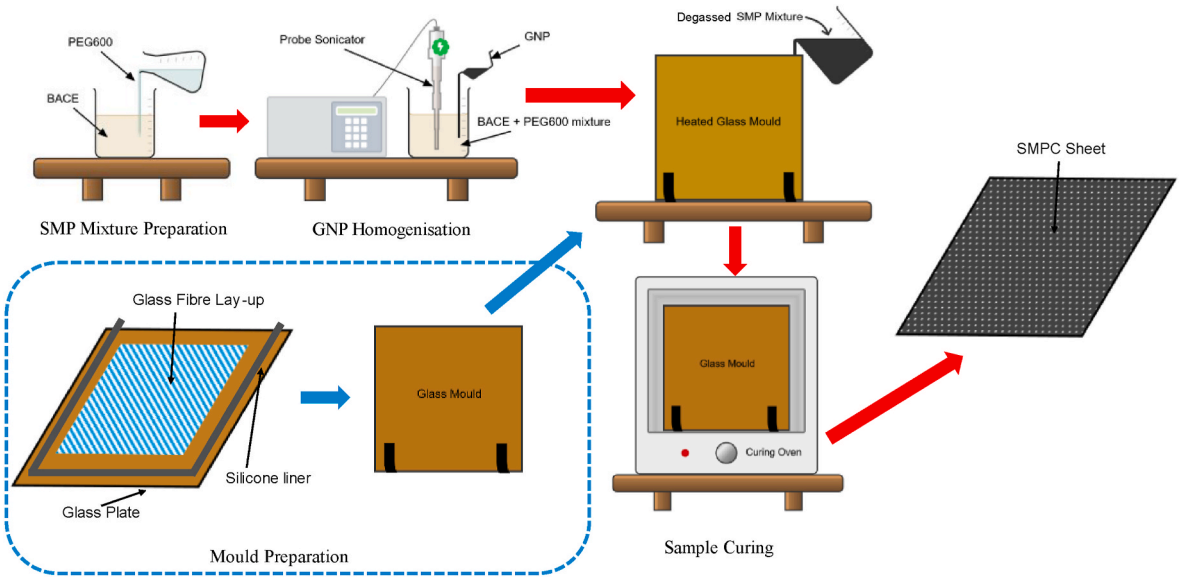

Fig. 1. SMPC fabrication flow chart.

120 °C for 5 h, at 180 °C for 2 h and at 210 °C for 5 h. Finally, SMPC sheets with 3 mm thickness and ~18 % fibre volume fraction were obtained, and specimens were cut per the ASTM/ISO standards (details mentioned in each test procedure) using a waterjet cutter.

2.1.3. Fabrication of the SMPC specimens

SMPC with the three 0/90° and three ±45° sandwich glass fibre layout configurations were fabricated with and without GNP. Neat SMP and GNP-filled SMP samples were also fabricated as controlled samples for the thermo-mechanical property comparison (Table 1). Glass Fibre (GF) lay-ups were arranged as shown in Fig. 2(a). Microscopic images of the fibre lay-ups are shown in Fig. 2(b).

2.2. Atomic oxygen exposure test

SMPC samples were exposed to Atomic Oxygen with the use of the AO interaction facility available at the National Space Test Facility (NSTF), Australian National University, Canberra. GTX and NTX samples with and without GNP were exposed to AO to study the effect of adding GNP as a thermal filler. First, SMPC sheets with the dimensions of 220 × 122.25 mm^2 were fixed into the custom-made Aluminium sample holder to avoid AO exposure to the surfaces except for the top surface. Samples were kept inside the plasma chamber as shown in Fig. 3 and then they were exposed to AO plasma (Fig. 3) with a flux of 5.46 × 10^{14} atoms/cm^2.s in 30 Pa (~99 % vacuum/0.3 mbar) of pressure at room temperature. Initially, samples were weighed and then kept under the AO exposure for 24 h continuously. After weighing for the second time, samples were exposed to another 24 h and then the final weights were taken. Overall, 48 h of AO exposure to the SMPCs according to the set parameters in the plasma chamber is equal to 300 days of AO exposure in a 550 km lower earth orbit [37]. Samples with the dimensions of 10 × 10 mm^2 test pieces were cut from the exposed SMPC for characterization and morphology tests with FTIR and SEM, respectively. The rest of the

Table 1
SMP and SMPC sample nomenclature and glass fibre lay-up configuration.

Sample Name	Sample Specifications	0/90° GF layers	±45° GF layers
N	Neat SMP	0	0
G	SMP +0.6 % GNP	0	0
NTX	SMP + GF Layers	3	3
GTX	SMP +0.6 % GNP + GF Layers	3	3

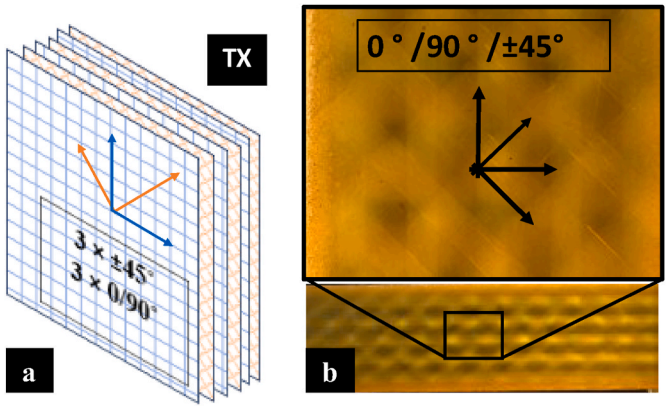

Fig. 2. (a) SMPC glass fibre lay-up configuration and (b) microscopic image of NTX samples with visible 0/90° and ±45° fibre lay-ups.

AO-exposed SMPC sheets were cut into standard samples with water jet cutting for thermomechanical properties using the DMA, mechanical properties with tensile and flexure tests and shape memory property tests.

2.3. Vacuum thermal aging test

The vacuum aging test was carried out using a Labec vacuum oven in 11.15 kPa (~89 % vacuum/111.46 mbar) at 140 °C. GTX SMPC samples were used for the vacuum thermal aging test and each set of samples was kept from 1 to 4 weeks under above mentioned conditions. Vacuum-aged SMPC samples were tested for the change in their chemical structure, thermomechanical property, tensile property and shape memory behaviour. Afterwards, the results were compared with control SMPC samples.

2.4. Material characterization and mechanical property evaluation

The changes that happened to the SMPC before and after different exposures were tested using a few methods. The changes to the chemical structure of the polymer and the morphology were measured using FTIR analysis and then using microscopic and SEM image analysis, respectively. The thermomechanical and mechanical property changes were

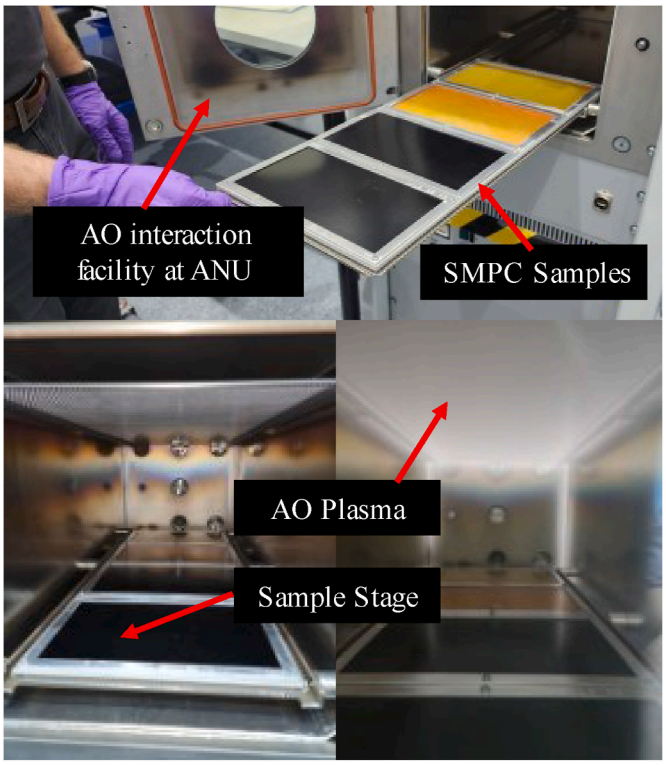

Fig. 3. Atomic Oxygen interaction facility and SMPC samples before and during AO exposure.

tested using Dynamic Mechanical Analysis (DMA) and then using tensile and flexural tests, respectively. The results of these tests can provide an accurate prediction of the durability of the developed SMPC in terms of the chemical, thermomechanical and morphological stability of the SMP matrix. ATR-FITR analysis was conducted using SHIMADZU IRAffinnity-1S equipment to identify the chemical structure changes. SMPC samples with the dimensions of 10 × 10 mm^2 were used for this scan in the spectrum range of 3000–450 cm^{-1} with an 8 cm^{-1} resolution and 5 scan times. Dynamic mechanical analysis (DMA) of the SMPCs was performed using TA Instruments hybrid rheometer (Discovery HR-2) under ASTM D7028 standard. Specimens were tested using the dual cantilever fixture with 1 Hz frequency, 25 μm axial displacement and temperature ramp of 5 °C/min from 25 to 220 °C. Each SMP sample was tested, and their storage modulus and tan(δ) behaviours were analysed. The storage onset temperature (T_s) of the graph was taken as the primary T_g value since the stability of the storage modulus was critical for the applications of the SMPCs. However, tan(δ) peak temperature (T_δ) was considered as the secondary T_g value since it is important to determine the shape programming and recovery temperature.

The surface morphology of the SMPCs before and after AO exposure was initially observed with LEICA DMS300 and Olympus DSX1000 high-definition microscopes. Then in-depth observations were carried out using ZEISS EVO 18 scanning electron microscopy (SEM) at an acceleration voltage of 10 kV after coating the SMPC surfaces with gold. Further analysis of the SEM images was carried out with Gwyddion 2.64 SPM data visualisation and analysis tool.

Mechanical properties of a material play a crucial role in the application designing stage. As a load-bearing and shape-changing material in a micro-gravity environment (e.g., pressure vessel, release mechanism), understanding the tensile and flexural behaviour of a material is important. Therefore, the tensile and flexural properties of vacuum-aged and AO-exposed SMPCs were tested using an MTS 100 kN uni-axial tensile testing machine according to ASTM D638–22 and ASTM 790–17 standards, respectively. Samples with dimensions of 25 mm × 250 mm with a crosshead speed of 2 mm/min were used for the uniaxial tensile test. The gauge length of the used extensometer was 25 mm, and the strain data were measured separately to the crosshead displacement. Equations mentioned in section A2.25 were used to calculate the stress and strain. Young's modulus of the samples was calculated using the trendline drawn for the strain measured using the extensometer. Flexural properties were measured using the samples with the dimensions of 13 mm × 70 mm and using 2 mm/min crosshead speed. The flexural stress, strain and modulus were calculated according to the equations mentioned in section 12 of the used standard. Furthermore, the effect of increasing temperature on the SMPCs was studied by testing the tensile and flexural properties of the NTX and GTX samples using an MTS 10 kN uni-axial tensile testing machine with an attached environmental chamber. Samples were tested at 25, 100, 120 and 140 °C for their high-temperature mechanical properties.

Finally, a suitability analysis is carried out to calculate the limitations of the developed GTX SMPC. "Section VIII Rules for Construction of Pressure Vessels" by the American Society of Mechanical Engineers (ASME) was used for this suitability analysis. Equations from the sub section UG-27(3) (ASME VIII) [38] for a hemispherical dish end, thin wall pressure vessels were used for this calculation.

2.5. Shape memory effect evaluation

The fold-deploy test method [39] was used to calculate shape fixity (R_f) and recovery (R_r) ratios using equations (1) and (2). SMPC samples were heated and bent using the environmental chamber attached to the MST 10 kN tensile machine [40]. First, the chamber was heated up to ~T_δ (170 °C) at a rate of 5 °C/min. During the R_f evaluation [35], SMPC samples were kept at ~ T_δ (170 °C) for 15 min in the environmental chamber and bent 75 ± 6° with a diameter of 12 mm three-point bending setup at a 1 mm/min crosshead speed (Fig. 4(a)) and the fixed angles were measured using a DAR-200 digital angle ruler (Fig. 4 (b)). After that, SMPCs were reheated, the recovery process was monitored at the mentioned temperatures, and the R_r was calculated. SMPC $R_{r,20\text{-}220}$ were calculated by keeping the SMP strips at 20, 40, 60, 80, 100, 120, 140,160, 180, 200, and 220 °C for 30 min inside the oven, respectively.

$$R_f = \frac{\theta_{fixed}}{\theta_{max}} \times 100\% \quad (1)$$

$$R_r = \frac{\theta_{fixed} - \theta_{end}}{\theta_{max}} \times 100\% \quad (2)$$

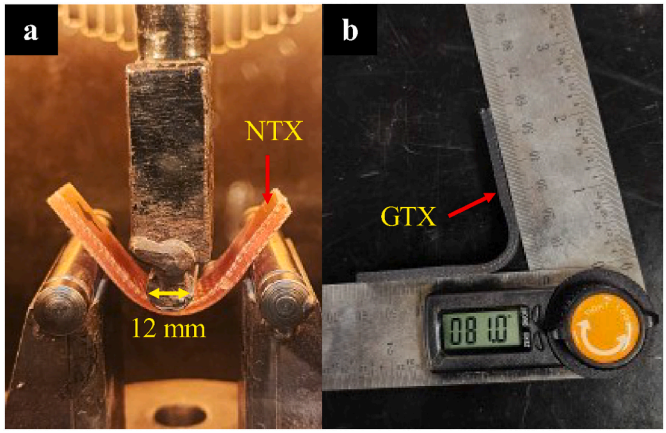

Fig. 4. (a) Shape fixation at 75 ± 6 °C inside the environmental chamber and (b) shape fixity and recovery angle measurement by digital angle ruler.

3. Results and discussion

3.1. Morphological and chemical structure changes

3.1.1. Surface morphology of AO-exposed SMPCs

Changes after 48 h of AO exposure on GTX and NTX were visible to the naked eye, and they are depicted in Fig. 5 (a & c). Digital microscope images from both low (Fig. 5(a & c)) and high-definition microscopic images in Fig. 5(b & d) shows severe erosion on the SMPC surfaces. Due to the AO exposure-induced erosion, mass losses in GTX and NTX were measured as 0.4 g and 0.5 g, respectively. Further analysis done with the SEM images of AO-exposed GTX and NTX shows the AO-induced surfaces in detail (Fig. 6). Using Gwyddion 2.64 SPM data visualisation and analysis tool, first multiple images were cropped into 25 × 30 μm^2 areas, image surface data were levelled by the mean plane subtraction option and then the 3D views of the image data were generated. Dimensions of the groves were measured using the distance measuring tool and the groove density was calculated manually. According to the analysed images, both GRX and NTX showed grooves created by AO (Fig. 6(c & f)). While the grooves in GTX are ~1 μm wide with a distribution of ~0.24 grooves/μm^{-2}, NTX shows ~0.63 μm wide groves with a distribution of ~0.46 grooves/μm^{-2}. Furthermore, GTX shows shallow depth of grooves at ~92 nm and NTX shows deeper grooves at ~142 nm. According to these values, AO exposure has given GTX ~54.35 % less erosion and a smoother surface after 48 h compared to NTX. Even though erosion due to AO is inevitable, surface morphology differences in GTX and NTX clearly show that the added GNP has acted as a barrier to AO protecting the polymer matrix from further erosion.

The further erosion protection of the developed Cyanate ester-based SMPC can be achieved by adding protective coatings [41] on the GNP-filled SMPC to AO erosion can be explained through several factors. AO attacks the materials by diffusion. Yet, according to the studies [42–44] even small amounts of GNP can significantly reduce gas permeability in polymer films by 50–500 times. This improvement comes from the well-dispersed GNP achieved by the sonication process during the SMPC fabrication stage. Since GNP is essentially impermeable and has a large surface area and high aspect ratio, it creates a twisting, labyrinthine path for the AO atoms to travel through the SMP matrix. This complex pathway makes it much harder for the AO to reach and erode the underlying Triazine and Isocyanurate structure compared to a neat SMP structure.

3.1.2. FTIR analysis of vacuum thermal aged and AO-exposed SMPCs

To analyse the chemical structure changes to AO exposed and vacuum thermal aged SMPCs, an FTIR analysis was carried out and shown in Fig. 7. FTIR spectrums show the existence of Isocyanurate at 1465 cm^{-1} and 1720 cm^{-1} through the (O═C─N) transmittance groups as well as the Triazine rings through the peaks at 1357 cm^{-1} and 1550 cm^{-1}. Furthermore, peaks induced from (─C─O─C─) and (─CH_2─) groups, respectively at 1072 cm^{-1} and 2862 cm^{-1} show the existence of PEG. An (─O─C≡N) group-induced peak can also be seen at 2360 cm^{-1} (Fig. 7(a)) in NTX samples due to remaining uncured cyanate ester groups [45].

According to Fig. 7(a), AO has not affected the chemical structure of the SMPC. Even after 48 h of AO exposure, above mentioned groups remain unchanged in terms of their peak intensity due to the high bond energy (over 2000 kJ/mol) of the Isocyanurate and Triazine groups [31]. If the Oxygen atom hits the polymeric surface with enough energy, it can bond with carbon atoms on the polymeric surface. However, if another AO atom strikes this bond, the -C-*O*-C- will break from the rest of the structure eroding the surface further [46]. This can be mentioned as the reason for the unchanged chemical structure in AO-exposed SMPCs.

Interestingly, the peak at 1720 cm^{-1} induced by the carboxyl groups of Isocyanurate has increased in intensity over the 4 weeks. Isocyanurate is one of the two key groups responsible for the stable Cyclcomatrix structure of Cyanate Ester SMP which increased the thermomechanical stability of the polymer [34]. This can be due to the post-curing effect that happens in the SMP matrix during thermal aging, and it can be mentioned as the only chemical reaction during the vacuum aging process. However, due to lower bond energy, peaks (2862 cm^{-1} and 1072 cm^{-1}) induced by PEG seem to be reduced in intensity over the 4 weeks. This can be due to the degradation of PEG crosslinks at high

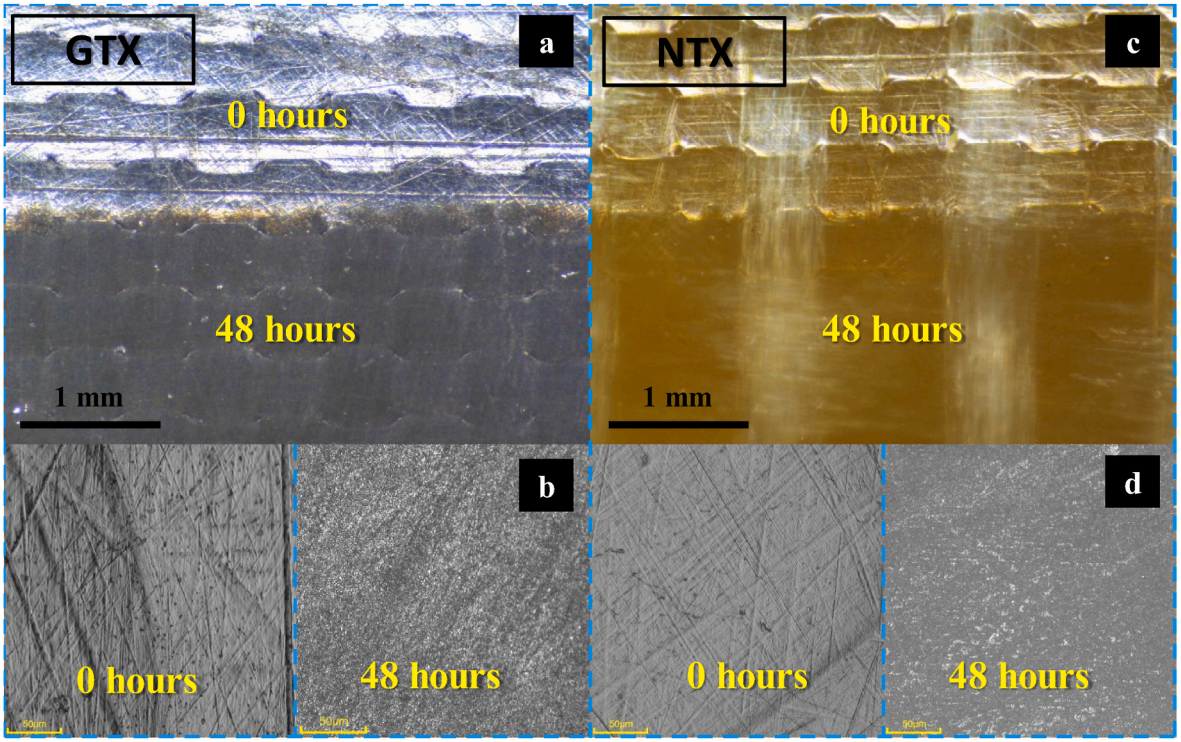

Fig. 5. AO exposed GTX samples (a),(b) and NTX samples (c),(d) under Leica and Olympus microscopes, respectively.

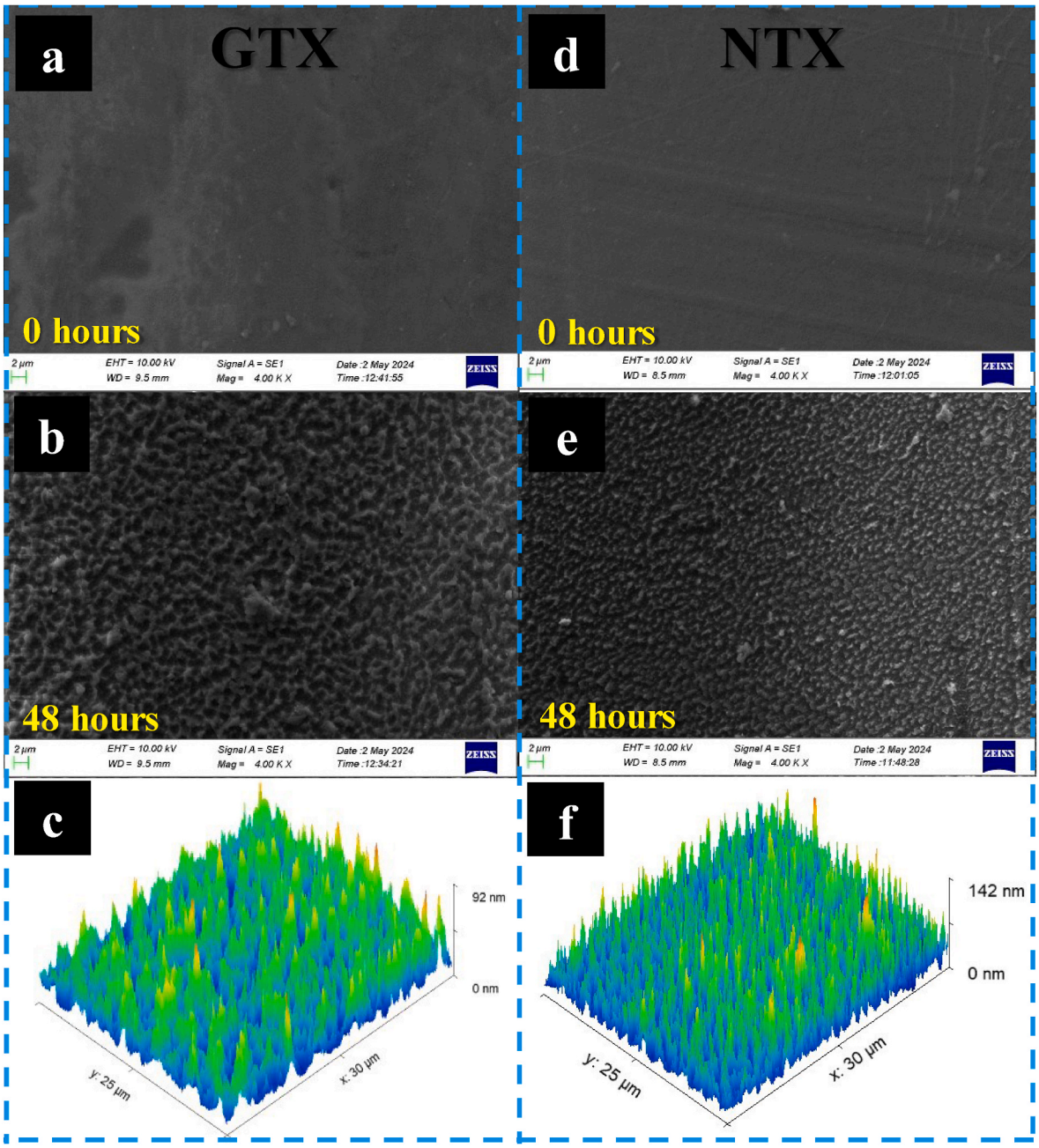

Fig. 6. (a),(d) Unexposed GTX and NTX samples. (b),(e) AO exposed GTX and NTX samples. (c),(f) Surface roughness analysis of GTX and NTX after 48 h of AO exposure.

temperatures. This behaviour is also discussed in section 3.2.

Overall, AO has not significantly affected the chemical structure of the SMP. Yet, vacuum thermal aging for 4 weeks at 140 °C has affected the SMP by breaking PEG chains leading to further thermomechanical, mechanical and shape memory property changes. This will be further discussed in the next sections.

3.2. Thermomechanical property analysis

Storage modulus and tan(δ) behaviour of SMPs and SMPCs were analysed to identify the variation after adding GNP, glass fibres, the effect of AO exposure and vacuum aging. The addition of GNP has resulted in an increase of storage modulus in 0.19 GPa and kept them over the whole temperature range (Fig. 8(a)). This can be mainly due to GNP obstructing the polymer chain movements. However, Kaftelen-Odabşı H. et al. (2022) [47] show that the increased amounts of graphene can drop the storage modulus values due to uneven dispersion of graphene in the matrix. This is further explained by the tensile and flexural behaviour of the NTX and GTX SMPCs in section 3.3.

Interestingly, the addition of glass fibre layers to the SMP resulted in around 2 GPa increment of storage modulus at room temperature as well as more stable storage modulus behaviour with increasing temperature (Fig. 8(a)). This effect has been studied and demonstrated by Mohan T. et al. (2023) [48] and Song P. et al. (2024) [49]. Furthermore, Tan(δ) half peak width ($S_{1/2}$) remains in the region between 27.8 ± 0.43 to 32.99 ± 0.31 °C (Table 2). This shows the addition of GNP and fibre has not affected on uniformity of the network structure of the SMP severely. However, the area under the Tan(δ) peak reduced from 31.61 ± 0.51 to 20.31 ± 0.11 °C in N and NTX, respectively decreasing the relaxation ability of the fibre-reinforced SMPC. It is important to emphasise that

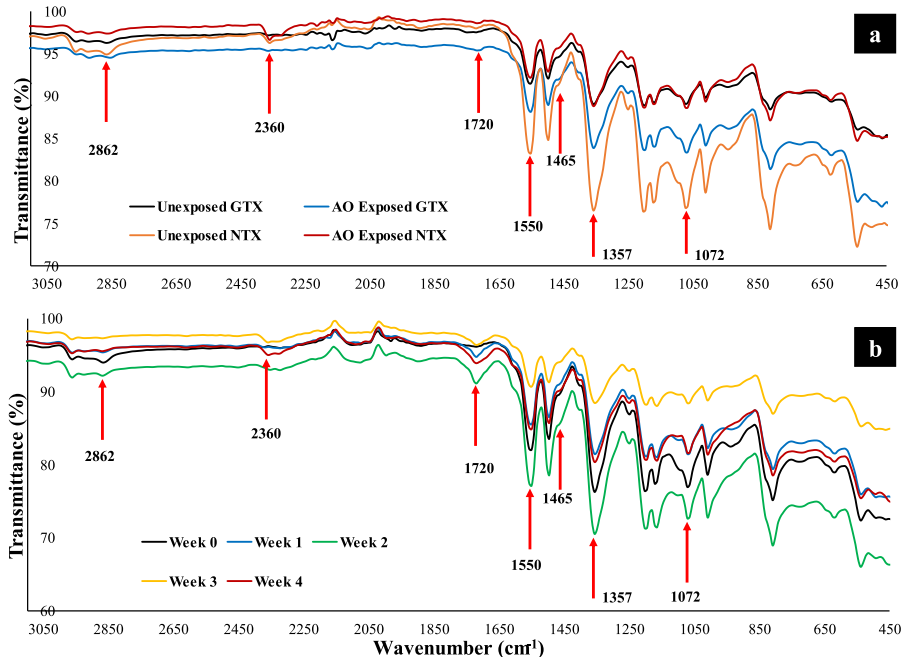

Fig. 7. FTIR spectrum of (a) vacuum thermal aged GTX samples and (b) AO exposed/unexposed SMPC samples.

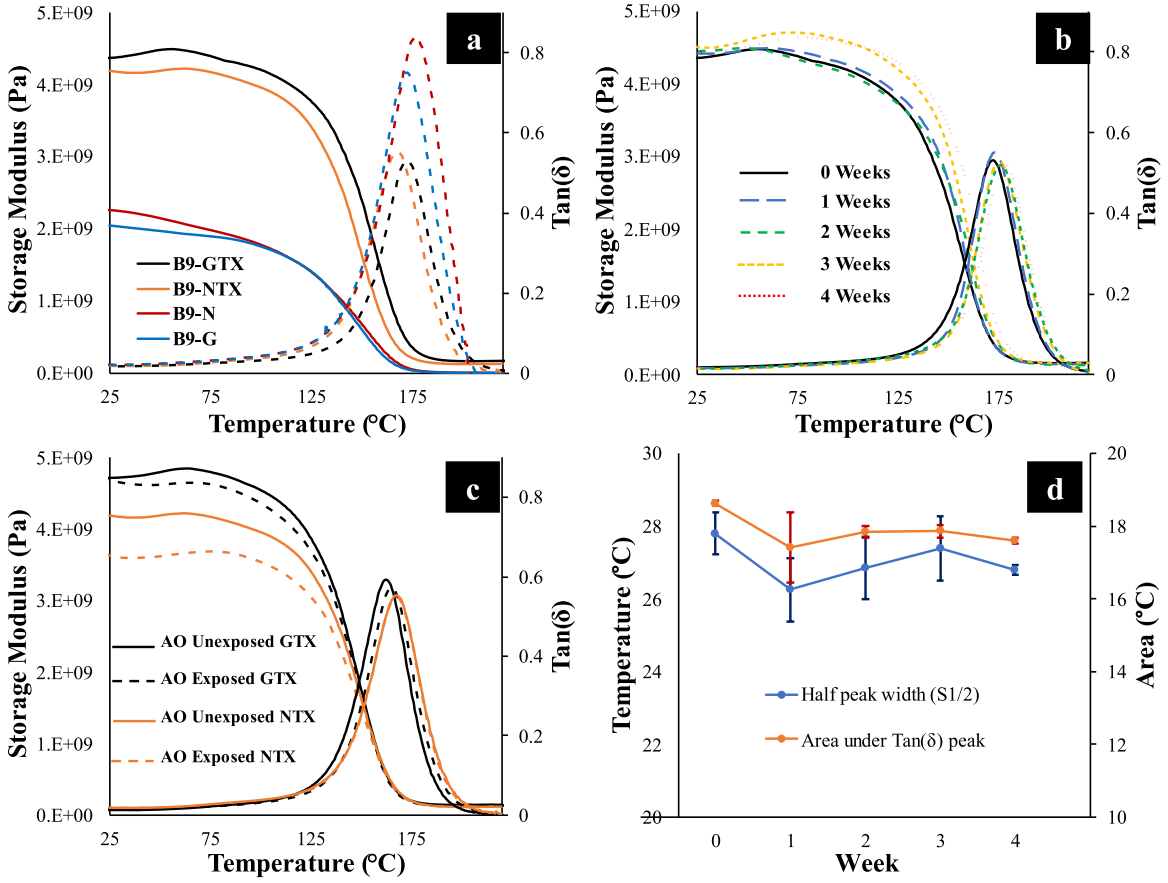

Fig. 8. DMA graphs of (a) controlled and unexposed SMP and SMPC samples, (b) vacuum-aged GTX samples and (c) AO exposed/unexposed SMPC samples. (d) Tan (δ) analysis of vacuum thermal aged GTX samples.

Table 2
T_g and Tan(δ) analysis of the SMPs and SMPCs.

SMP/SMPC Sample	T_s (Storage Onset)/°C	T_δ (Tan(δ) peak)/°C	Tan(δ) half peak width ($S_{1/2}$)/°C	Area under Tan(δ) peak/°C
N	129.99 ± 0.35	175.91 ± 0.50	32.99 ± 0.31	31.61 ± 0.51
G	125.01 ± 0.25	171.97 ± 0.36	32.29 ± 0.25	28.69 ± 0.28
NTX	130.23 ± 1.12	168.04 ± 1.10	29.10 ± 0.33	20.31 ± 0.11
AO Exposed NTX	124.54 ± 1.87	167.72 ± 0.13	30.22 ± 0.06	20.16 ± 0.08
GTX	131.68 ± 1.79	169.01 ± 0.62	27.80 ± 0.58	18.63 ± 0.07
AO Exposed GTX	128.69 ± 0.69	165.11 ± 0.32	27.16 ± 0.43	19.98 ± 0.51
GTX Week 0	131.68 ± 1.79	169.01 ± 0.62	27.80 ± 0.58	18.63 ± 0.07
GTX Week 1	138.86 ± 1.62	173.03 ± 0.69	26.26 ± 0.87	17.42 ± 0.97
GTX Week 2	141.22 ± 0.67	175.60 ± 0.09	26.85 ± 0.86	17.84 ± 0.16
GTX Week 3	140.37 ± 2.77	176.14 ± 0.29	27.38 ± 0.88	17.86 ± 0.18
GTX Week 4	142.67 ± 3.63	178.05 ± 0.63	26.79 ± 0.14	17.60 ± 0.07

the addition of fibres can be considered a suitable answer to the storage modulus stability problem faced by many cyanate ester based SMPs.

The storage modulus and Tan(δ) behaviour of AO exposed and unexposed NTX and GTX samples are graphed in Fig. 8(c). Even though, the Tan(δ) behaviour of both SMPCs remains relatively unchanged in the region from 165.11 ± 0.32 °C to 169.01 ± 0.62 °C (Table 2), the storage modulus behaviour of NTX has been severely affected by the AO exposure dropping by ~0.56 GPa over the temperature range until ~125 °C. Furthermore, NTX shows a higher T_s (storage onset) drop of 5.69 °C compared to GTX (2.99 °C) after 48 h of AO exposure. The addition of GNP as a barrier to less erosion and structural changes in the SMP matrix can be mentioned as the reason for this behaviour.

After going through four weeks of vacuum thermal aging, GTX samples from each week were tested for their thermomechanical behaviour and DMA graphs were drawn as shown in Fig. 8(b). GTX samples showed an increase in storage onset T_s values from 131.68 ± 1.79 °C to 142.67 ± 3.63 °C and Tan(δ) peak T_δ from 169.01 ± 0.62 °C to 178.05 ± 0.63 °C. This can be due to the thermal aging-induced PEG chain session at high temperatures over a long period. Interestingly, after the first week of vacuum aging, storage onset shows relatively stable values over the next 3 weeks (Table 2). Furthermore, $S_{1/2}$ and the area under Tan(δ) peak remains relatively unchanged (Fig. 8(d)) showing the stability of the polymer network structure. Due to that, it is safe to assume, that only PEG crosslinks are affected during the vacuum thermal aging process compared to thermally stable isocyanurate and triazine structures [32] in the SMPC. According to Cao S. et al. (2011) [50] and Xu X. et al. (2019) [51] storage modulus behaviour with increasing temperature is proportional to Young's modulus of the polymer materials. Since GTX SMPC shows stable storage modulus (3.75 ± 0.15 GPa at 130 °C in week 0) even after vacuum thermal aging (3.8 ± 0.4 GPa at 130 °C in week 4), shows the thermomechanical stability of the SMPC. From the perspective of the load-bearing application at higher temperatures, this behaviour is favourable once the SMPC has recovered and performed its primarily designed function since the SMPC will become much more stable in the high-temperature region without losing its other required properties.

3.3. Mechanical property analysis

3.3.1. High-temperature behaviour of the SMPCs

The tensile and flexural behaviour of the SMPCs were tested and analysed at elevated temperatures, before and after AO exposure and vacuum-thermal aging. Since the design temperature of the SMPCs lies at 130 °C, the mechanical properties were evaluated until 140 °C. The initial Young's modulus of 7.91 GPa is reduced to 1.4 GPa at 140 °C in the GTX samples and 7.43 GPa is reduced to 1.04 GPa at 140 °C in the NTX samples (Fig. 9 (a & b)). Furthermore, the maximum stress of the GTX and NTX samples at 140 °C was calculated as 52.06 MPa (118.54 ± 3.35 MPa at 25 °C) and 46.98 MPa (133.49 ± 2.11 MPa at 25 °C), respectively. The maximum stress drops in GTX and NTX were 56.08 % and 64.81 %, respectively. However, the flexural stress drop (from 25 °C to 140 °C) of GTX and NTX shows similar percentages of 68.73 % and 69.72 %, respectively (Fig. 10 (a & b)). Moreover, once the SMPCs reached 120 °C and the maximum flexural stress, their deflection movement kept going without an increasing load (Fig. 10(c & d)). In comparison, GTX SMPCs are not severely affected by added GNP concerning the mechanical behaviour of NTX SMPCs. Excellent dispersion of GNP into the voids of the SMP network structure can be mentioned as the reason for this behaviour. Furthermore, these results are important for the designing stage of the applications considering different service temperatures.

3.3.2. Effect of AO exposure and vacuum thermal aging on the mechanical properties

According to the tensile behaviour of AO-exposed SMPCs (Fig. 9(d) and Table 3), both NTX and GTX show similar behaviour in terms of Young's modulus and maximum strain. However, GTX shows a higher drop of maximum stress at 29.07 % compared to a 7.21 % drop in NTX. On the other hand, the maximum flexural stress of AO-exposed GTX increased from 11.5 % compared to a decrease of 1.7 % in NTX (Fig. 10 (e)). Overall, both tensile and flexural modulus are decreased to some extent (Tables 3 and 4) after the AO exposure. Even though the maximum tensile stress of GTX was reduced, its maximum flexural stress has been increased.

The effect of vacuum thermal aging on GTX was tested and tensile graphs were drawn for each week (Fig. 9(c)). According to Table 5, the mechanical properties of the GTX SMPCs are affected by a 3.29 % increase in Young's modulus, 26.3 % decreased maximum stress and 15.6 % decreased maximum strain over 4 weeks. Interestingly, it was noted that all the above mechanical properties were either stabilized or slightly increased over time. This can be due to the degradation of more heat susceptible PEG crosslinks and thermally stable Isocyanurate and Triazine structures.

3.4. Shape memory effect analysis

The shape memory behaviour of the SMPC samples was studied by analysing the shape fixity (R_f) and shape recovery (R_r) percentages. NTX and GTX samples showed 100 % shape fixity ratios during shape programming. Both NTX and GTX samples stayed under 10 % of R_r at 140 °C as a requirement for application development (Fig. 11(a, b & c)). The rapid shape recovery started around the Tan(δ) T_g values of each SMPC. However, GTX shows higher and quicker shape recovery behaviour compared to NTX samples (Fig. 11(a & b)). This can be due to higher thermal conductivity influenced by GNP in GTX samples.

In terms of shape memory behaviour within the AO-exposed SMPCs, NTX was mostly affected. Compared to the AO-exposed GTX samples, NTX shows a delayed recovery (Fig. 11(a) with increasing temperature. Before the AO exposure, GTX and NTX showed 27.64 % and 17.04 % shape recovery at 160 °C. After the AO exposure, GTX showed 19.42 % shape recovery while NTX dropped to 7.06 % shape recovery at 160 °C. Even though both shape recovery percentages have dropped, GTX SMPC has shown better performances compared to the NTX SMPC. This can be

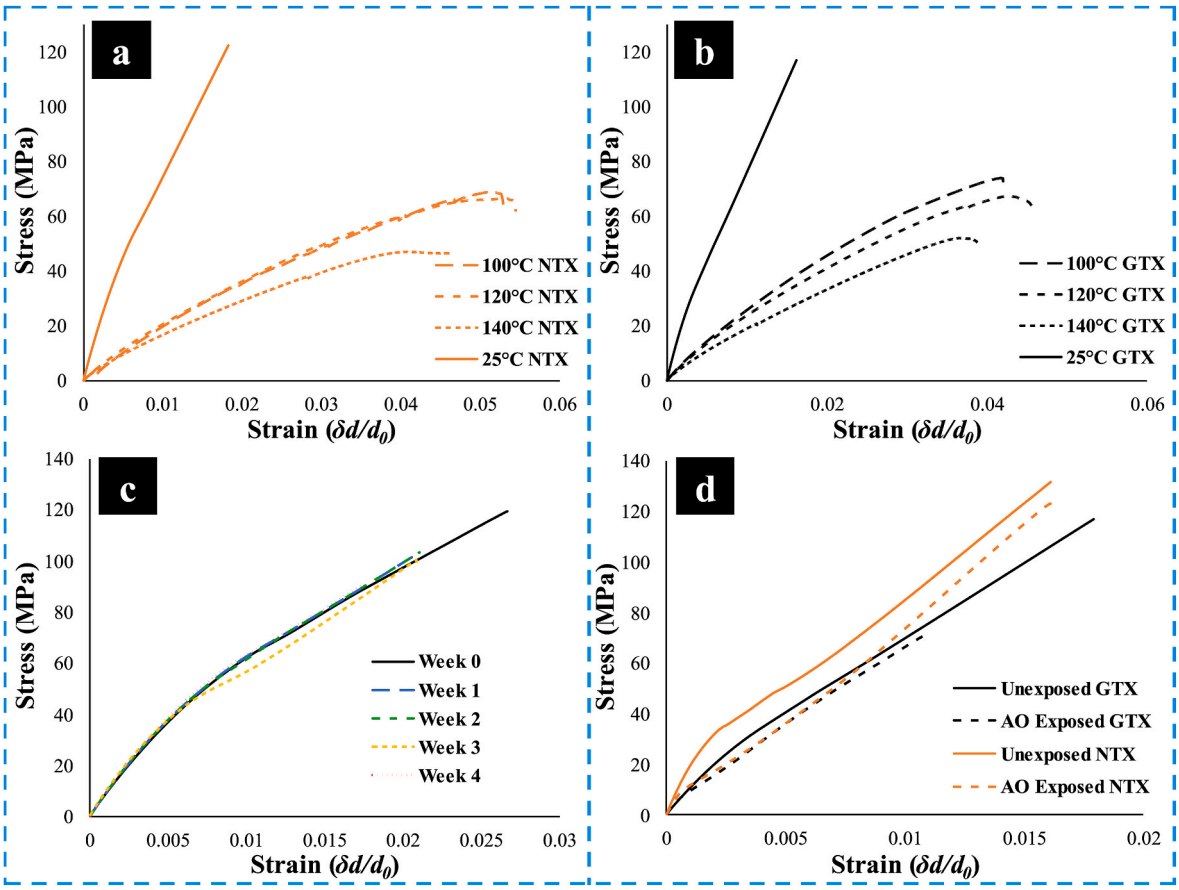

Fig. 9. Tensile behaviour of (a) NTX and (b) GTX at high temperatures. (c) Effect of vacuum thermal aging on the tensile behaviour of GTX samples. (d) Tensile behaviour of AO exposed/unexposed SMPC samples.

due to less surface erosion on GTX due to GNP, protecting the PEG crosslinks within and inheriting higher thermal conductivity.

Further proving the degradation of PEG crosslinks in the SMPC matrix, vacuum thermal aged GTX samples showed a drop in shape recovery efficiency over the 4 weeks (Table 6). The R_r of 31.17 % at 160 °C of the initial GTX SMPCs has dropped to 8.23 % at the same temperature after 4 weeks of vacuum thermal aging (Fig. 11(c)). In a study done by Ping Z. et al. (2023) [32] shows no adverse effect on the shape fixity and recovery properties in the BACE SMP after vacuum thermal cycling. However, these SMP samples were kept at 170 °C for 50 h maximum with the thermal cycling between −170 °C and +170 °C. Therefore, thermal degradation/chain scission of PEG crosslinks over time can be mentioned as the reason for this significant delay in shape recovery.

Another important aspect to consider during the shape memory behaviour of the developed SMPC is the damage to the fibres and the matrix during shape programming and recovery. This has been experimentally evaluated by Jayalath S et al. (2024) [36]. According to that GTX samples have shown a 48.7 % drop in maximum tensile strength after the shape recovery due to fibre slippage Fig. 11(d). However, depending on the programmed angle, programmed temperature and the programmed rate, the incurred damage can be varied.

3.5. Suitability analysis of the SMPC for the orbital and lunar thin wall structures

After evaluating the performances of the developed SMPC, a suitability analysis of the material as a good candidate for space and lunar applications can add value to this study. As one of the possible designs of dwelling units, the hemispherical dish end thin wall pressure vessel was considered to calculate the maximum inner diameter of a hemispherical thin wall made from the developed SMPC. According to the property analysis done in the previous sections, the mechanical properties of the GTX SMPC are at their weakest at 140 °C. Calculation of the dimensions of a pressure vessel with 101,325 Pa (1 atm) internal pressure with its weakest properties can set a benchmark for further development of the material as well as possible applications. UG-27(3) (ASME VIII) equations (Eq:3, 4 & 5) [38,52,53] were used for the calculation by considering the worst-case scenarios (Table 7) such as the maximum stress at 140 °C, safety factors, and join efficiency of the composites. 385.8 mm (Eq:3), 776.3 mm (Eq:4) and 777.69 mm (Eq:5) were calculated as the maximum internal diameter of the cylindrical shell and hemispherical shell of the pressure vessel that can be achieved using the GTX SMPC. Even though these dimensions are not enough for human dwelling units, this diameter can be further increased by adding more fibre layers or different fibres such as carbon, Kevlar or basalt fibres to the composite and increasing the thickness. Furthermore, micro-gravity in the LEO and the moon (1.62 ms^{-2}) and stabilising mechanical properties during the vacuum thermal aging process will enhance the stability of the structure further. As a dwelling unit, additional protective layers will be added [54] to protect the structure from debris, charged particles, and temperature fluctuations.

Cylindrical shell: circumferential stress

$$D_i = \frac{2t(SE - 0.6\,P)}{P} \tag{3}$$

Cylindrical shell: longitudinal stress

$$D_i = \frac{2t(2SE - 0.4\,P)}{P} \tag{4}$$

Spherical shell

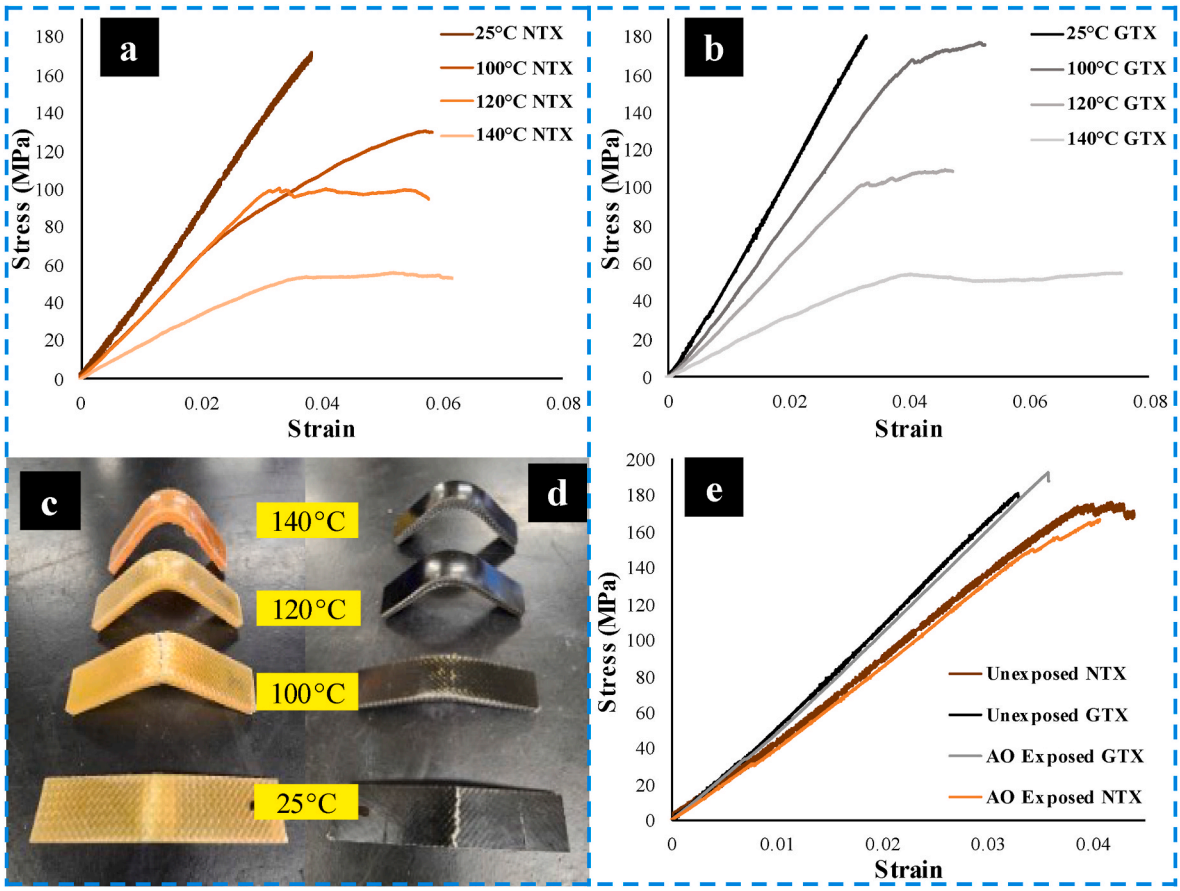

Fig. 10. Flexural behaviour of (a) NTX and (b) GTX at high temperatures. Bending ability of (c) NTX (d) GTX flexural samples at different temperatures. (e) Flexural behaviour of AO exposed/unexposed SMPCs.

Table 3
Young's modulus, max stress, and max train results of AO exposed/unexposed samples.

Sample	Young's modulus (GPa)	Max Stress (MPa)	Max Strain ($\delta d/d_0$)
Unexposed NTX	7.43 ± 0.14	133.49 ± 2.11	0.016 ± 0.001
AO Exposed NTX	7.23 ± 0.20	123.87 ± 1.03	0.014 ± 0.002
Unexposed GTX	7.91 ± 0.77	118.54 ± 3.35	0.045 ± 0.006
AO Exposed GTX	7.47 ± 0.33	84.08 ± 12.55	0.010 ± 0.000

Table 4
Flexural modulus, max flexural stress, and max flexural train results of AO exposed/unexposed samples.

Sample	Flexural modulus (GPa)	Max flexural Stress (MPa)	Max flexural Strain ($\delta d/d_0$)
Unexposed NTX	4.43 ± 0.14	170.81 ± 1.41	0.041 ± 0.004
AO Exposed NTX	4.06 ± 0.17	167.91 ± 6.21	0.056 ± 0.030
Unexposed GTX	5.59 ± 0.30	178.85 ± 0.76	0.033 ± 0.000
AO Exposed GTX	5.45 ± 0.37	199.42 ± 16.21	0.039 ± 0.004

Table 5
Young's modulus, max stress, and max train results of vacuum thermal aged GTX samples.

Sample	Young's modulus (GPa)	Max Stress (MPa)	Max Strain ($\delta d/d_0$)
Week 0	7.91 ± 0.77	118.54 ± 3.35	0.045 ± 0.006
Week 1	7.22 ± 1.05	77.01 ± 34.54	0.030 ± 0.013
Week 2	7.37 ± 1.24	76.13 ± 38.24	0.028 ± 0.009
Week 3	7.46 ± 1.26	74.19 ± 36.30	0.027 ± 0.009
Week 4	7.65 ± 0.16	87.36 ± 4.52	0.038 ± 0.028

$$D_i = \frac{2t(2SE - 0.2P)}{P} \quad (5)$$

3.6. Summary of the durability analysis

Two main durability tests and their effect were discussed throughout this discussion. Firstly, AO exposure has eroded both GNP-filled and unfilled SMPC. However, GNP-filled SMPC (GTX) showed less susceptibility with a groove depth of ~92 nm to AO erosion compared to the NTX samples (~142 nm groove depth). Even though there are no changes in the chemical structure after the AO exposure, the storage modulus, mechanical properties, and shape recovery of NTX showed a higher drop compared to the property drop in GTX samples (Table 2, Table 3, Table 4 and Fig. 11(a&b)).

The vacuum thermal aging over 4 weeks has affected the SMP chemical structure due to the thermal decomposition of PEG crosslinks. This is identified from the reduction of the 2862 and 1027 cm^{-1} FTIR spectrum peak reduction over the 4 weeks. The storage onset and tan(δ) temperature increase (Table 2), Young's modulus increase (from 3.29

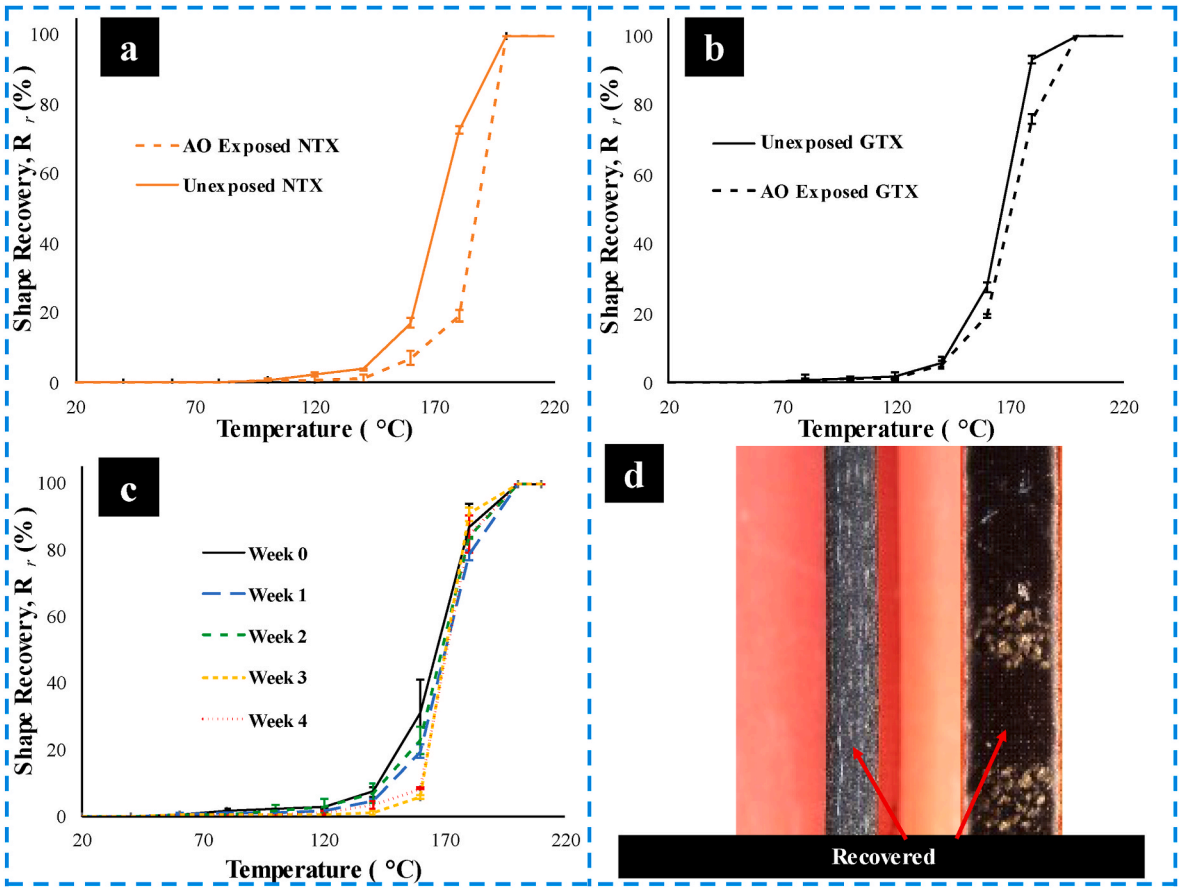

Fig. 11. Shape recovery behaviour of AO exposed and unexposed (a)NTX samples and (b) GTX samples. (c) Shape recovery behaviour of vacuum thermal aged GTX samples. (d) Before and after shape recovery of GTX samples [36].

Table 6
Shape recovery behaviour of vacuum thermal aged GTX samples over the 4 weeks.

Temperature (°C)	Shape Recovery Percentage				
	Week 0	Week 1	Week 2	Week 3	Week 4
20	0.00 ± 0.00	0.00 ± 0.00	0.00 ± 0.00	0.00 ± 0.00	0.00 ± 0.00
40	0.00 ± 0.00	0.00 ± 0.00	0.00 ± 0.00	0.00 ± 0.00	0.00 ± 0.00
60	0.31 ± 0.43	0.30 ± 0.42	0.18 ± 0.13	0.05 ± 0.06	0.18 ± 0.25
80	1.30 ± 0.88	0.66 ± 0.93	0.45 ± 0.25	0.05 ± 0.06	0.27 ± 0.37
100	1.84 ± 0.54	0.75 ± 0.80	1.63 ± 1.41	0.05 ± 0.06	0.27 ± 0.37
120	2.47 ± 0.37	1.62 ± 0.13	2.98 ± 2.19	0.05 ± 0.06	1.06 ± 0.63
140	7.23 ± 1.37	4.48 ± 0.36	6.95 ± 2.99	1.11 ± 0.52	3.26 ± 1.11
160	31.17 ± 9.52	19.47 ± 2.11	22.83 ± 3.97	5.58 ± 0.70	8.23 ± 0.10
180	86.72 ± 7.06	78.59 ± 1.52	84.17 ± 0.02	90.73 ± 1.77	84.70 ± 5.53
200	100.00 ± 0.00	100.00 ± 0.00	100.00 ± 0.00	100.00 ± 0.00	100.00 ± 0.00

%), and maximum strain decrease (from 15.6 %) over 4 weeks also strengthen the above fact since the fewer amounts of PEG crosslinks increased the storage modulus stability of the SMP and increased its brittleness [34].

Table 7
Considered parameters for the calculation.

Parameters	Values
SMPC Thickness (*t*)	3 mm
Internal Pressure (*P*)	101,325 Pa (1 atm)
Maximum Tensile Stress of GTX SMPC (S) at 140 °C (worst-case scenario)	52.6 MPa
Safety factor for long-term static pressure (for composite materials)	4
Joint efficiency (E) (worst-case scenario)	0.5

4. Conclusion

In this research work, the durability of the cyanate ester-based SMPC was evaluated under extreme service environments in space such as elevated temperatures, vacuum thermal environment and AO exposure separately. The effect of added GNP into the SMPC matrix was also evaluated under elevated temperatures and AO exposure. A suitability analysis was also done to determine the ability to construct a thin wall structure using the developed SMPC under worst-case scenarios. The following conclusions were drawn after testing for the morphological, chemical, thermomechanical, mechanical and shape memory changes of the SMPCs.

1. GNP added to GTX SMPC showed increased protection compared to NTX SMPCs against the AO exposure-induced micro-erosion.
2. While there is no significant change in the chemical structure of the SMPC due to AO exposure. Vacuum thermal aging has affected the

PEG crosslinks to be reduced. This has affected the thermo-mechanical, mechanical and shape memory properties of the SMPC.
3. The vacuum thermal aging induced stable thermo-mechanical and mechanical property stability is favourable to the long-term service of the SMPC once the shape memory effect-related application is done.
4. The shape memory effect of GNP-added GTX SMPCs showed better shape recovery ability compared to NTX SMPCs even after the AO exposure.
5. Developed GTX SMPC specifications were suitable for constructing thin shell pressure vessels closer to 0.4–0.8 m in diameter and higher dimensions are possible increasing the number of fibre lay-ups, the thickness of the composite, and using high-strength fibres.

Overall, GNP has acted as a good thermal conductive filler while active as a protective material for AO exposure-induced erosion. Even though, AO exposure-induced surface erosion is unavoidable, fabricated SMPC survived 300 days in a 550 km LEO orbit without significantly changing the thermo-mechanical, mechanical and shape memory properties. For longer service time, a protective coating on the SMPC components is recommended. Vacuum thermal aging also showed favourable behaviours in GTX and NTX with stable mechanical properties over the exposed time. Finally, developed Cyanate ester-based SMPC has shown comparatively stable thermo-mechanical and mechanical properties in addition to excellent shape memory properties even after exposure to extreme conditions. Therefore, developed SMPC can be undoubtedly suggested for load-bearing-deployable thin wall components that can withstand multidirectional stresses. Thin shell structural components (for dwelling units) that can be programmed to save storage space in payload fairings and then can be deployed during construction are another important application suitable for the developed SMPC. In addition, further tests are warranted to study the synergistic effects including cryogenic temperatures, long-term materials degradation and thermal cycles on the SMPC before the component and structure design stage. Future developments and tests such as testing the effect of different dispersion variabilities of GNP, the effect of protective coatings on the SMPC for the AO exposure, light activation methods, complex shape programming for structural parts such as hemispherical shells and cylindrical shells can be done. Challenges such as cost, resource efficiency and compliance with safety standards should be addressed for the long-term sustainability of the SMPC-based space applications.

CRediT authorship contribution statement

Sandaruwan Jayalath: Writing – original draft, Methodology, Investigation, Formal analysis, Data curation, Conceptualization. **Eduardo Trifoni:** Supervision, Resources. **Jayantha Epaarachchi:** Writing – review & editing, Supervision. **Madhubhashitha Herath:** Writing – review & editing, Supervision. **Eleftherios E. Gdoutos:** Supervision. **Bandu Samarasekara:** Supervision.

Declaration of competing interest

The authors declare that they have no known competing financial interests or personal relationships that could have appeared to influence the work reported in this paper.

Data availability

Data will be made available on request.

Acknowledgement

The authors would like to thank for the support given by the staff in the National Space Test Facility (NSTF), ANU, Canberra. Further, the authors would like to extend their gratitude to Dr Hizam Rusmi (Senior Research Technical Officer), Dr Mazhar Peerzada (Senior Research Technical Officer), Mr Oliver Kinder (Senior Technical Officer) and Mr Nathan Strenzel (Technical Officer) at the University of Southern Queensland, and Mr Mihiranga Jayaweera (Technical Officer) at the University of Moratuwa, Sri Lanka, for their valuable assistance in this research.

References

[1] L. Luo, F. Zhang, L. Wang, Y. Liu, J. Leng, Recent advances in shape memory polymers: multifunctional materials, multiscale structures, and applications, Adv. Funct. Mater. 34 (2024) 1–32, https://doi.org/10.1002/adfm.202312036.
[2] B.C. Kholkhoev, K.N. Bardakova, A.N. Nikishina, Z.A. Matveev, Y.M. Efremov, A. A. Frolova, A.A. Akovantseva, E.N. Gorenskaia, N.A. Verlov, P.S. Timashev, V. F. Burdukovskii, 4D-printing of mechanically durable high-temperature shape memory polymer with good irradiation resistance, Appl. Mater. Today 36 (2024) 102022, https://doi.org/10.1016/j.apmt.2023.102022.
[3] M. Herath, J. Epaarachchi, M. Islam, L. Fang, J. Leng, Light activated shape memory polymers and composites: a review, Eur. Polym. J. 136 (2020) 109912, https://doi.org/10.1016/j.eurpolymj.2020.109912.
[4] H. Hassan, H. Hallez, W. Thielemans, V. Vandeginste, A review of electro-active shape memory polymer composites: materials engineering strategies for shape memory enhancement, Eur. Polym. J. 208 (2024) 112861, https://doi.org/10.1016/j.eurpolymj.2024.112861.
[5] Y. Zou, W. Guo, X. Lu, Z. Sun, L. Li, A novel water-induced two-way shape memory polymer based on poly (L-lactic acid)/silk fibroin composites, Compos. Commun. 46 (2024) 101822, https://doi.org/10.1016/j.coco.2024.101822.
[6] K.D.C. Emmanuel, L.H.J. Jeewantha, H.M.C.M. Herath, J.A. Epaarachchi, T. Aravinthan, Shape memory polymer composite circular and square hollow members for deployable structures, Compos. Part A Appl. Sci. Manuf. 171 (2023) 107559, https://doi.org/10.1016/j.compositesa.2023.107559.
[7] H.M.C.M. Herath, J.A. Epaarachchi, M.M. Islam, J. Leng, Carbon fibre reinforced shape memory polymer composites for deployable space habitats, Eng. J. Inst. Eng. Sri Lanka. 52 (2019) 1, https://doi.org/10.4038/engineer.v52i1.7323.
[8] J. Jeewantha, S. Jayalath, C. Emmanuel, M. Herath, E. Forster, M. Islam, J. Leng, J. Epaarachchi, Shape memory polymer smart plaster for orthopaedic treatments, Smart Mater. Struct. 31 (2022) 115016, https://doi.org/10.1088/1361-665X/ac943b.
[9] C. Zeng, L. Liu, Y. Du, M. Yu, X. Xin, P. Xu, F. Li, L. Wang, F. Zhang, Y. Liu, J. Leng, Space-deployable device based on shape memory cyanate ester composites, Compos. Commun. 42 (2023) 101690, https://doi.org/10.1016/j.coco.2023.101690.
[10] F.F. Li, Y.J. Liu, J.S. Leng, Progress of shape memory polymers and their composites in aerospace applications, Yuhang Xuebao/Journal Astronaut. 41 (2020) 697–706, https://doi.org/10.3873/j.issn.1000-1328.2020.06.007.
[11] B.C. Kholkhoev, A.N. Nikishina, K.N. Bardakova, Z.A. Matveev, D.A. Sapozhnikov, Y.M. Efremov, P.S. Timashev, V.F. Burdukovskii, 4D-printing of high-temperature shape-memory polymers based on polyimide, N,N-dimethylacrylamide and photoactive cross-linkers, Polymer (Guildf) 299 (2024) 126978, https://doi.org/10.1016/j.polymer.2024.126978.
[12] Z. Tang, J. Gong, P. Cao, L. Tao, X. Pei, T. Wang, Y. Zhang, Q. Wang, J. Zhang, 3D printing of a versatile applicability shape memory polymer with high strength and high transition temperature, Chem. Eng. J. 431 (2022) 134211, https://doi.org/10.1016/j.cej.2021.134211.
[13] J. Jin, X. Sun, D. Yu, Z. Chen, Research on ground microgravity simulation system based on parallel mechanism, Microgravity Sci. Technol. 36 (2024) 1–22, https://doi.org/10.1007/s12217-023-10094-5.
[14] Z. Song, C. Chen, S. Jiang, J. Chen, T. Liu, W.H. Deng, F. Lin, Optimization analysis of microgravity experimental facility for the deployable structures based on force balance method, Microgravity Sci. Technol. 32 (2020) 773–785, https://doi.org/10.1007/s12217-020-09807-x.
[15] M. Higgins, H. Benaroya, Utilizing the Analytical Hierarchy Process to determine the optimal lunar habitat configuration, Acta Astronaut. 173 (2020) 145–154, https://doi.org/10.1016/j.actaastro.2020.04.012.
[16] I. Gkolias, J. Daquin, F. Gachet, A.J. Rosengren, From order to chaos in Earth satellite orbits, Astron. J. 152 (2016) 119, https://doi.org/10.3847/0004-6256/152/5/119.
[17] K.K. de G. Finckenor, M. Miria, Space Environmental Effects, 2009, pp. 521–527, https://doi.org/10.1201/9781420084320-c27.
[18] H. Benaroya, The lunar environment, in: Build. Habitats Moon, Springer International Publishing, Cham, 2018, pp. 42–84, https://doi.org/10.1007/978-3-319-68244-0_3.
[19] E. Grossman, I. Gouzman, Space environment effects on polymers in low earth orbit, Nucl. Instrum. Methods Phys. Res. Sect. B Beam Interact. Mater. Atoms 208 (2003) 48–57, https://doi.org/10.1016/S0168-583X(03)00640-2.
[20] H.J. Fincannon, Lunar Environment and Lunar Power Needs, 2020, pp. 1–5.
[21] Y. Li, D. Lau, Advances in shape memory polymers and their composites : from theoretical modeling and MD simulations to additive manufacturing. https://doi.org/10.1016/j.giant.2024.100277, 2024.
[22] Y. Ma, H. Guo, Y. Xu, P. Li, W. Xu, J. Ji, Y. Shi, Effect of curing temperature on shape memory properties of graphene oxide-carbon fiber hybrid-reinforced shape

memory polymer composites, Polym. Compos. 45 (2024) 2140–2155, https://doi.org/10.1002/pc.27909.
[23] Y. Yang, X. Chen, B. Liu, Y. Li, H. Yin, Shape memory polymer composite supports for reinforcement binding: design, manufacturing, and validation, J. Reinforc. Plast. Compos. (2024) 1–17, https://doi.org/10.1177/07316844231225337.
[24] K. Mirasadi, D. Rahmatabadi, I. Ghasemi, M. Khodaei, M. Baniassadi, M. Bodaghi, M. Baghani, 3D and 4D printing of PETG–ABS–Fe3O4 nanocomposites with supreme remotely driven magneto-thermal shape-memory performance, Polymers 16 (2024), https://doi.org/10.3390/polym16101398.
[25] M. Gowri, N. Latha, M. Rajan, in: M.R. Maurya, K.K. Sadasivuni, J.-J. Cabibihan, S. Ahmad, S. Kazim (Eds.), Fiber- and Fabric-Reinforced Shape-Memory Polymers BT - Shape Memory Composites Based on Polymers and Metals for 4D Printing: Processes, Applications and Challenges, Springer International Publishing, Cham, 2022, pp. 267–286, https://doi.org/10.1007/978-3-030-94114-7_12.
[26] A. Kandelbauer, Cyanate ester resins, in: Handb. Thermoset Plast., Elsevier, 2022, pp. 587–617, https://doi.org/10.1016/B978-0-12-821632-3.00004-X.
[27] H.T.S. Jayalath, M. Herath, J. Epaarachchi, Cyanate esters as a high performing shape memory polymer: a review, Mater. Today Proc. 57 (2022) 693–700, https://doi.org/10.1016/j.matpr.2022.02.121.
[28] S.C. Arzberger, N.A. Munshi, M.S. Lake, J. Wintergerst, S. Varlese, M.P. Ulmer, Elastic memory composite technology for thin, lightweight, space- and ground-based deployable mirrors, in: W.A. Goodman (Ed.), Opt. Mater. Struct. Technol., 2003, p. 143, https://doi.org/10.1117/12.507157.
[29] S.C. Arzberger, M.L. Tupper, M.S. Lake, R. Barrett, K. Mallick, C. Hazelton, W. Francis, P.N. Keller, D. Campbell, S. Feucht, D. Codell, J. Wintergerst, L. Adams, J. Mallioux, R. Denis, K. White, M. Long, N.A. Munshi, K. Gall, Elastic memory composites (EMC) for deployable industrial and commercial applications, in: E. V. White (Ed.), Smart Struct. Mater. 2005 Ind. Commer. Appl. Smart Struct. Technol., 2005, p. 35, https://doi.org/10.1117/12.600583.
[30] F. Xie, L. Liu, X. Gong, L. Huang, J. Leng, Y. Liu, Effects of accelerated aging on thermal, mechanical and shape memory properties of cyanate-based shape memory polymer: I vacuum ultraviolet radiation, Polym. Degrad. Stabil. 138 (2017) 91–97, https://doi.org/10.1016/j.polymdegradstab.2017.03.001.
[31] F. Xie, X. Gong, L. Huang, L. Liu, J. Leng, Y. Liu, Effects of accelerated aging on thermal, mechanical, and shape memory properties of a cyanate-based shape memory polymer: II atomic oxygen, Polym. Degrad. Stabil. 186 (2021) 109515, https://doi.org/10.1016/j.polymdegradstab.2021.109515.
[32] Z. Ping, F. Xie, X. Gong, L. Liu, J. Leng, Y. Liu, Effects of accelerated aging on thermal, mechanical and shape memory properties of cyanate-based shape memory polymer: III vacuum thermal cycling, Polymers 15 (2023) 1893, https://doi.org/10.3390/polym15081893.
[33] S. Jayalath, M. Herath, J. Epaarachchi, E. Trifoni, E.E. Gdoutos, L. Fang, Durability and long-term behaviour of shape memory polymers and composites for the space industry - a review of current status and future perspectives, Polym. Degrad. Stabil. 211 (2023) 110297, https://doi.org/10.1016/j.polymdegradstab.2023.110297.
[34] S. Jayalath, M. Herath, J. Epaarachchi, E. Trifoni, E.E. Gdoutos, B. Samarasekara, Cyanate ester and polyethylene glycol based high temperature resistant shape memory polymer development for space applications, React. Funct. Polym. 201 (2024) 105949, https://doi.org/10.1016/j.reactfunctpolym.2024.105949.
[35] K.D.C. Emmanuel, H.M.C.M. Herath, L.H.J. Jeewantha, J.A. Epaarachchi, T. Aravinthan, Thermomechanical and fire performance of DGEBA based shape memory polymer composites for constructions, Construct. Build. Mater. 303 (2021) 124442, https://doi.org/10.1016/j.conbuildmat.2021.124442.
[36] S. Jayalath, J. Epaarachchi, M. Herath, Lay-up configuration of glass fibre on cyanate ester based shape memory polymer composites, 11th Australas. Congr. Appl. Mech. (2024). https://search.informit.org/doi/10.3316/informit.T202404160000999099079369178.
[37] J. Mathew, E. Trifoni, J. Ashby, S. Rosset, I.A. Anderson, LEO atomic oxygen interaction experiments at the ANU national space test facility, Proc. Int. Astronaut. Congr. IAC. 2022-Septe (2022) 18–22.
[38] The American Society of Mechanical Engineers, BPVC SECTION VIII Rules for construction of pressure vessels division 1 2023. https://www.asme.org/codes-standards/find-codes-standards/bpvc-viii-1-bpvc-section-viii-rules-construction-pressure-vessels-division-1/2023/print-book, 2023.
[39] R. Biju, C.P.R. Nair, Effect of phenol end functional switching segments on the shape memory properties of epoxy-cyanate ester system, J. Appl. Polym. Sci. 131 (2014), https://doi.org/10.1002/app.41196 n/a-n/a.
[40] K.D.C. Emmanuel, L.H.J. Jeewantha, H.M.C.M. Herath, J.A. Epaarachchi, T. Aravinthan, Damage onset analysis of optimized shape memory polymer composites during programming into curved shapes, Materialia 26 (2022) 101599, https://doi.org/10.1016/j.mtla.2022.101599.
[41] C. Huang, R. Huang, Y. Cheng, L. Zhao, N. Hu, Q. Wei, Strong and flexible MXene-based nanocomposite films for atomic oxygen resistance and electromagnetic interference shielding, Compos. Sci. Technol. 253 (2024) 110665, https://doi.org/10.1016/j.compscitech.2024.110665.
[42] G. Choudalakis, A.D. Gotsis, Permeability of polymer/clay nanocomposites: a review, Eur. Polym. J. 45 (2009) 967–984, https://doi.org/10.1016/j.eurpolymj.2009.01.027.
[43] W. Zhang, M. Yi, Z. Shen, X. Zhao, X. Zhang, S. Ma, Graphene-reinforced epoxy resin with enhanced atomic oxygen erosion resistance, J. Mater. Sci. 48 (2013) 2416–2423, https://doi.org/10.1007/s10853-012-7028-4.
[44] V. Singh, D. Joung, L. Zhai, S. Das, S.I. Khondaker, S. Seal, Graphene based materials: past, present and future, Prog. Mater. Sci. 56 (2011) 1178–1271, https://doi.org/10.1016/j.pmatsci.2011.03.003.
[45] K.S. Santhosh Kumar, A.K. Khatwa, C.P. Reghunadhan Nair, High transition temperature shape memory polymers (SMPs) by telechelic oligomer approach, React. Funct. Polym. 78 (2014) 7–13, https://doi.org/10.1016/j.reactfunctpolym.2014.02.008.
[46] D. Fugett, Atomic Oxygen Considerations for LEO De-orbit Trajectories Using Solar Sails, California Polytechnic State University, 2017. https://www.proquest.com/docview/2838440278?pq-origsite=gscholar&fromopenview=true&sourcetype=Dissertations&Theses.
[47] H. Kaftelen-Odabaşı, A. Odabaşı, M. Özdemir, M. Baydoğan, A study on graphene reinforced carbon fiber epoxy composites: Investigation of electrical, flexural, and dynamic mechanical properties, Polym. Compos. 44 (2023) 121–135, https://doi.org/10.1002/pc.27031.
[48] T.P. Mohan, K. Kanny, Dynamic mechanical analysis of glass fiber reinforced epoxy filled nanoclay hybrid composites, Mater. Today Proc. 87 (2023) 235–245, https://doi.org/10.1016/j.matpr.2023.05.282.
[49] P. Song, D.J. Chapman, A.M. Graham, B. Lukić, A. Rack, C.R. Siviour, Thermomechanical characterisation of a thermoplastic polymer and its short glass fibre reinforced composite: influence of fibre, fibre orientation, strain rates and temperatures, Compos. Part A Appl. Sci. Manuf. 180 (2024), https://doi.org/10.1016/j.compositesa.2024.108099.
[50] S. Cao, X. Wang, Z. Wu, Evaluation and prediction of temperature-dependent tensile strength of unidirectional carbon fiber-reinforced polymer composites, J. Reinforc. Plast. Compos. 30 (2011) 799–807, https://doi.org/10.1177/0731684411411002.
[51] X. Xu, C. Koomson, M. Doddamani, R.K. Behera, N. Gupta, Extracting elastic modulus at different strain rates and temperatures from dynamic mechanical analysis data: a study on nanocomposites, Composites, Part B 159 (2019) 346–354, https://doi.org/10.1016/j.compositesb.2018.10.015.
[52] A.K. Jha, An optimum design of pressure vessel using ASME (BPVC) sec-VIII div-I, II and ASME (BPVC) sec-II part-A, Int. J. Res. Appl. Sci. Eng. Technol. 8 (2020) 1670–1682, https://doi.org/10.22214/ijraset.2020.5272.
[53] Y. Xing, Burst pressure design of the cargo tank used in a novel large subsea freight-glider, IOP Conf. Ser. Mater. Sci. Eng. 1201 (2021) 012014, https://doi.org/10.1088/1757-899x/1201/1/012014.
[54] A.S. Howe, C.B. Mechanism, D.S. Habitat, E. Control, E.M. Campaign, E. Activity, H.D. Unit, I.S. Station, L.E. Orbit, L.S. Decelerator, M.A. Vehicle, N. Aeronautics, P. E. Vehicle, R.A. Frames, Space Exploration, 2015, pp. 1–24.